Recent Insights into the Physics of the Sun and Heliosphere:
Highlights from SOHO and Other Space Missions
IAU Symposium, Vol. 203, 2001
P. Brekke, B. Fleck, and J. B. Gurman eds.

Three Dimensional image Reconstruction of an Hα Flare

Z. Q. Qu, Y. C. Jiang, T. Luan and Z. Xu

Yunnan Astronomical Observatory, Chinese Academy of Sciences, Kunming 650011, China

National Astronomical Observatories, Chinese Academy of Sciences, Beijing 100012, China

Abstract. The three-dimensional (3D) image of an Hα flare is reconstructed from its line-center and seriary off-center filtergrams. The reconstruction is based on the principle of the line formation theory that the contribution function (CF) of emergent specific line intensity describes the escape photon distribution from stellar atmospheric layers. Thus the reconstruction depends on the model atmosphere accepted which determines the CF. An Hα flare taking place on April 22, 1992 is utilized to illustrate the process.

Keywords: line formation – radiative transfer – solar flares

1. Introduction

It is well known that different wavelength points within a spectral line may form in different depth regions in stellar atmosphere. From the simulated observation of line formation process (cf Qu et al., 1999, hereafter Paper I), it is found that even for the escape photons with one definite wavelength, the filtergram is generally not an image of a narrow layer, say, it may be a mixture of two seperate regions. Thus the 3D image recontruction is really redistributing the escape photons to the layers according to the escape photon distribution function - the contribution function of line intensity.

2. Contribution function, model atmosphere of flare and calculation of line parameter

We adopt the CF expressed by equation (17) of Paper I. That is

$$CF_I(\tau_k) = e^{-\tau_{k-1}}[(1-e^{-\Delta\tau_{k-1}})S_t(\tau_k) + (1-e^{-\Delta\tau_{k-1}}-\Delta\tau_{k-1})\frac{dS_t(\tau_k)}{d\tau}]. \quad (1)$$

where CF_I denotes the CF of emergent specific line intensity I. The meanings of the other symbols can be found in Paper I.

Because the flare considered below was a bright flare, the Model F2 (with 32 grids) of Machado et al (1980) is accepted. Additional grids for this model

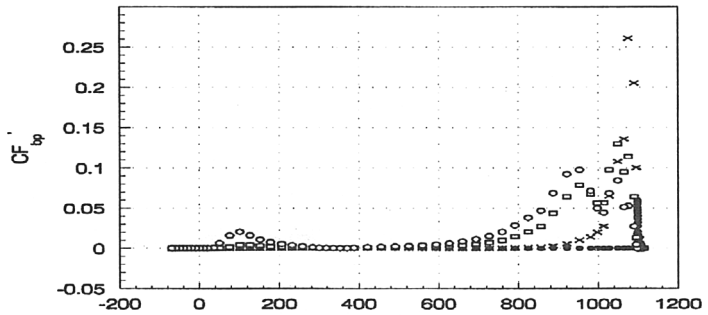

Figure 1. CF_{bp} curves of the bandpasses describing the distribution of the escape photons. They are obtained according to Eq.(3). The discrete solid circles represent the fractional contribution of the escape photons within the band with central wavelength locating at line center from each depth layer, the crosses with central wavelength at $\pm 0.5\mathring{A}$, the open square at $\pm 1.0\mathring{A}$ and finally the open circles with central wavelength at $\pm 1.5\mathring{A}$. The width of bandpass is $0.5\mathring{A}$.

are interpolated according to the trend of the parameter curve so that 99 grids in total are given while the geometric height range is a little shortened from ($1120km$, $-75km$) to ($1114.80km$,$-69.29km$).

The calculation code of line parameters, i.e., damping constant a, Doppler width $\Delta\lambda_D$, line-center and continuum absorption coefficients χ_l and χ_c, and line-center and continuum emission coefficients j_l and j_c, is proposed by Ding and Fang (1989). They considered the hydrogen atomic structures to 12 energy levels plus one continuum state.

3. Hα escape photon distribution of the used bandpasses in the bright flare case

In actual observation, the filtergrams are acquired within a bandpass $\Delta\lambda_{bp}$ rather than a single wavelength point. The corresponding CF_{bp} can be defined as

$$CF_{bp}(z) = \int_{\lambda_{0,bp}-1/2\Delta\lambda_{bp}}^{\lambda_{0,bp}+1/2\Delta\lambda_{bp}} CF(\lambda, z)d\lambda/\Delta\lambda_{bp}. \quad (2)$$

Where $\lambda_{0,bp}$ denotes the central wavelength of the bandpass. When normalized as

$$CF'_{bp}(z) = CF_{bp}(z)/\int_{z_0}^{z_n} CF_{bp}(z)dz, \quad (3)$$

the CF can be regarded as the weight factor of the escape photons with the wavelengths within the bandpass from height interval $z + dz$, while the line spectrum is formed by the wavelength distribution of the total amount of the escape photons coming from all the involved layers. In the above expression, z_0 is the bottom level adopted by the model atmosphere and z_n the top one. Fig.1 plots the CF'_{bp} curves of these bandpasses used by the Solar Structure Telescope (SFST) mounted at our observatory, which are signified by their central wavelengths.

https://doi.org/10.1017/S0074180900219372 Published online by Cambridge University Press

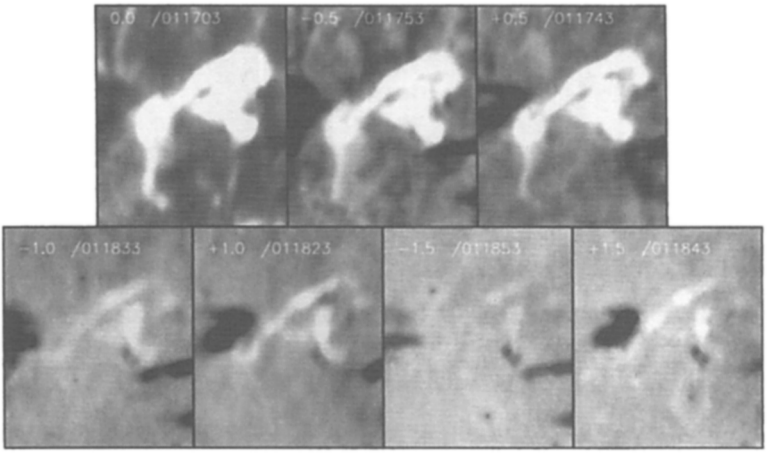

Figure 2. One set of filtering images of an Hα flare taking place on April 22, 1992 (NOAA4139). The first number in the upper-left corner of each panel indicates the central wavelength of the bandpass from the line center in unit of $\mathring{A}$ and the number following '/' shows the time when the image was acquired.

4. 3D image reconstruction of an Hα two-ribbon flare

The 3D image of an Hα flare only shows the lower part of the flare embedding in the chromosphere and even in the photosphere, or precisely, the part of the magnetic footpoints and their surrounding diffusion regions of hot plasma which are thermalized by the energetic electrons, protons and ions produced and accelerated by the release of magnetic energy.

We adopt one set of the line-center and off-center Hα filtergrams taken by the SFST. An Hα flare (NOAA7139) was observed from 010613UT to 035004UT, April 22, 1992. It, ranked optically 1N and M1.4 by X-ray, began at 01042UT after a filament blew away and reached its maximum at 01089UT and finally ended at 0152UT. The width of bandpass used is $0.5\mathring{A}$ and one set of observations were carried out with the central wavelengths locating respectively at the line center, $\Delta\lambda = \pm 0.5, \pm 1.0, \pm 1.5\mathring{A}$. Fig.2 shows the set of the filtergrams. These pictures were taken within 2 minutes, shorter than the rise phase duration.

The flare patches are drawn out by the evolution of the involved area. As usual, the flare kernels in the line center and $\pm 0.5\mathring{A}$ filtergrams show saturation and this will bring some distortion of the reconstructed 3D image.

Fig.3 is the reconstructed 3D images utilizing the 'Polyshade' plotting of the software IDL. It is worthy noting that this kind of plot only lends the profiles of the concerning structure but cannot show the different brightness within it. The images are a little smoothed. Fig.3a) represents the structure in the normal coordinates while it is also viewed in an angle with rotations respectively about 'Southeast' and 'Southwest' axes by 60° in panel b), and its side-view is depicted in panel c). Notice that to clearly see the stratification of the flare, the space along the height axis 'h' is 100 times extended than the other two axes. The tickmarks are $1''$ apart on both 'Southeast' and 'Southwest' axes.

https://doi.org/10.1017/S0074180900219372 Published online by Cambridge University Press

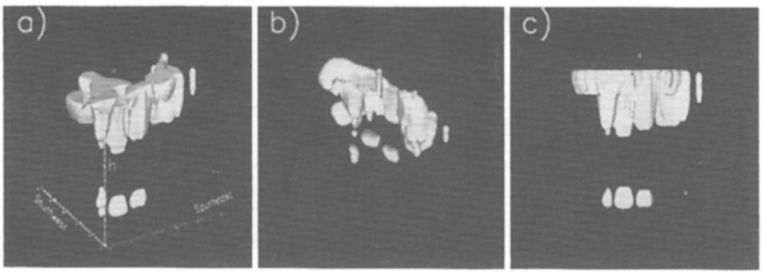

Figure 3. Reconstructed 3D images of an Hα flare taking place on April 22,1992 (NOAA4139) during its maximum.

The tooth-like structure originates from the fainter part in the flare patches and is shaped by the behaviour of the CF. On the other hand, the dark gap between the chromospheric part and the photospheric one is ascribed to the much less contribution from the temperature minimum region and its surrounding layers (see Fig.1).

5. Discussions

The 3D images of an Hα flare is shown based on the principle that the contribution function of the emergent intensity gives the layer distribution of the escape photons and thus the reconstruction of the 3D image is reconstracted by redistributing the escape photons received to the involved layers.

It is worthy noting that the reconstruction of the 3D image of the active region in the manner introduced is observation as well as model dependent. For the latter factor, the model atmosphere should be changed if one wants to reconstruct the 3D images in different phases for the whole process of energy release when a flare takes place. On the other hand, for the observation there are some aspects influencing the precision of the reconstructed 3D image. The most important one is the saturation frequently met in observation. Another concerns the bandpass used. The narrower it is, the finer the 3D image. Furthermore, if the period of acquiring the seriary filtergrams forming the source of the reconstructed 3D image lasts too long compared to the time variation scale in the active region, the reconstructed image will be far from the reality. The best way to solve this issue is to utilize a telescope which can aquire one set of data simultaneously.

Acknowledgments. This work is supported by the National Natural Science Foundation of China under grant number 19973016.

References

Ding, M.D. & Fang, C. 1989, A&A, 225, 204

Machado, M.E., Avrett, E.H., Vernazza, J.E., & Noyes, R.W. 1980, ApJ, 242, 336

Qu, Z.Q., Zhang, X.Y., & Gu, X.M. 1999, MNRAS, 305, 737